Available online at www.sciencedirect.com
SCIENCE DIRECT®
Journal of Magnetic Resonance 169 (2004) 203–214
JMR Journal of Magnetic Resonance
www.elsevier.com/locate/jmr

NMR relaxation and pulsed field gradient study of alginate bead porous media

Melanie M. Britton,[a,*] Robin G. Graham,[b] and Ken J. Packer[b]

[a] Department of Chemical Engineering, University of Cambridge, New Museums Site, Pembroke St., Cambridge CB3 2RA, UK
[b] Department of Chemistry, University of Nottingham, Nottingham, University Park NG7 2RD, UK

Received 11 December 2003; revised 21 April 2004
Available online 20 May 2004

Abstract

Experiments are presented, which correlate molecular displacement with the multi-exponential T_2 relaxation times of water flowing and diffusing through an alginate bead pack. Three systems were studied comprising beads of 3, 1 or <1 mm in diameter. T_2-resolved propagators were obtained through a combined pulsed gradient stimulated echo (PGSTE) and Carr–Purcell–Meiboom–Gill (CPMG) experiment. Fourier transformation with respect to **q** produces a propagator for each echo in the CPMG train. Inverse Laplace transformation of the CPMG decays for each point (Z) in the propagator produced a two-dimensional propagator. Analysis of these two-dimensional propagators provided insight into the transport and exchange behaviour of water flowing through this system. This experiment has been simulated in a model bead structure and the resulting T_2 relaxation time behaviour and T_2-resolved propagators were found to be in good agreement with the experimental data. We also present a theoretical analysis of the response to the combined PGSTE/CPMG sequence in the simple model case of Pouseille flow in a cylindrical capillary, where diffusion to a surface sink is assumed to be the dominant relaxation mechanism.

Keywords: Diffusion; Flow; Exchange; Relaxation; Two-dimensional; T2-displacement correlation; Laplace transform

1. Introduction

Nuclear magnetic resonance (NMR) has been widely used to characterise spatially heterogeneous systems through the relaxation behaviour or transport processes of fluids contained within. There are many types of such structurally heterogeneous systems and an understanding of the spatial distribution of fluids and their diffusion and flow within these structures is important in a variety of contexts. Examples can be found in the reservoir rocks and aquifers of the oil and water industries, in chromatographic separation materials, in biological tissues or food materials, and in many other naturally occurring or man-made systems. Typically the measured NMR properties of molecules in the probed fluid reflect the internal dimensions and geometries of these structures when the self-diffusion lengths or flow displacements, over timescales comparable with NMR spin relaxation times, are of a similar order to the structural scales.

There are two main types of NMR experiment which have been widely used in this way. First, measurement of relaxation data can reveal unique information [1,2] about systems consisting of spatially distributed regions of different intrinsic relaxation times which are sampled by self-diffusing or flowing spins. This problem was first addressed analytically by Brownstein and Tarr [3], who studied the multi-exponential relaxation decay found in biological cells. They studied the effects on relaxation behaviour of systems where spins diffused to a surface relaxation sink and showed how the multi-exponential nature of the relaxation was a consequence of this and was sensitive to the geometry of the cells. Investigations of multi-exponential relaxation have also been reported by Hills and co-workers [4] who studied a variety of systems including Sephadex [5] and glass [6,7] beads. These studies considered the effects of both surface and

* Corresponding author. Fax: +44-1223-334796.
E-mail address: mmb29@cam.ac.uk (M.M. Britton).

1090-7807/$ - see front matter © 2004 Elsevier Inc. All rights reserved.
doi:10.1016/j.jmr.2004.04.016

volume sinks. Experimental data were compared with numerical simulations based on two basic model structures, lamellar and a sphere in a cube.

The second main NMR method applied in the characterisation of heterogeneous systems is the pulsed magnetic field gradient spin echo (PGSE) technique. This method is usually used to measure the average propagator, $P_\Delta(\mathbf{R})$, which is the probability density for finding molecular (spin) displacements $\mathbf{R}$ in time Δ. For self-diffusion, the analysis of the propagator dependence on observation time Δ can lead to information concerning the pore structure being revealed [8,9]. In the case of externally driven flow, similarly, the evolution of the propagator reveals the influence of the structure on the flow field and dispersion processes, leading again to information on structural scales [10–12].

In the basic two pulse PGSE experiment, the propagator is obtained by Fourier transformation of the NMR signal $S_\Delta(\mathbf{q})$ with respect to $\mathbf{q}$, for a fixed observation time, Δ. Here the wavevector $\mathbf{q}$ is given by $\mathbf{q} = \gamma\delta\mathbf{g}/2\pi$, where γ is the magnetogyric ratio and $\mathbf{g}$ and δ are the gradient vector and duration, respectively. The upper limit on Δ is determined by the spin relaxation properties of the system, as all PGSE experiments take place against the background of the spin relaxation of the system under study. Where the transverse relaxation, T_2, times are short, such that $T_1/T_2 \gg 1$, a stimulated echo experiment can be used, which stores the magnetisation in the longitudinal direction for the greater part of the interval Δ, and is thus largely dependent on the longer longitudinal, T_1, relaxation time.

Whatever the form of the PGSE experiment there is always some effect on the derived propagator arising from differential relaxation characteristics in spatially separated regions. Most often, these relaxation effects are neglected or experiments are constrained to values of Δ for which relaxation effects may be shown to be small for the system under study. There have been investigations of the effects of relaxation on the determination of distance scales from PGSE experiments [13–15] and these show that strong surface relaxation, for example, causes the size scales to be underestimated. Work by Van As and co-workers [16] used combined CPMG and PGSE experiments to measure the diffusion coefficients for different T_2 components in biological tissue. Hills et al. [17] have also combined relaxation and diffusion measurements to measure the frequency dependence of the water diffusivity in a model porous medium. Experiments which correlate T_1–T_2 relaxation [18] relaxation–diffusion and diffusion–diffusion exchange [19,20] by means of two-dimensional inverse Laplace transformation have also recently been reported. However, none of these studies produced a direct correlation between relaxation and transport of the type reported here.

In this paper we report measurements of the relaxation, displacement, and diffusive-exchange behaviour of fluid in randomly packed alginate bead systems of three different mean bead diameters. Measurements of the transverse relaxation times show that there is not a simple relationship between relaxation components and physical regions within the system. Rather the relaxation distribution is additionally dependent on diffusive exchange, as the root mean square displacement of fluid molecules is of the order of the internal structural scales. These systems have further been explored through the application of a two-dimensional experiment [21], which correlates the relaxation properties of the fluid contained in both the pore space and hydrogel beads with displacement distributions arising from flow and diffusion. In this experiment the aim is to measure the joint probability density $P_\Delta\{Z;T_2\}$, which correlates displacements in one dimension with T_2 values. The same could be done for T_1 but as there is a negligible difference in T_1 between the fluid in the bead and pore, this experiment was not done. The determination of such correlations is of interest because, by associating T_2 values with a structural size scale, a relationship between local size scale and transport properties of the fluid can be established. Such information could provide valuable insight in a number of areas of research. For example, consider a system where the porosity may be distributed in a complicated manner, perhaps with regions of porosity having a small average pore scale adjacent to regions of larger pore dimensions. Here diffusion and flow will be directly related to the nature of this spatial distribution of pores [12,22] and the T_2 values will likewise often reflect the local pore scales [1,2]. Therefore correlations contained within the joint propagator, $P_\Delta\{Z;T_2\}$, will allow a more detailed understanding of the movement of fluid through the differently sized porosities. An example of such a system is a chromatographic support, where fluid is distributed in and around beads of insoluble polymers, or biological tissues, and where fluid flows and diffuses through organised compartments of differing scales and connectivity.

In addition to the experimental work carried out, these systems have also been modelled. Previous investigations [3,5,23], studying the relaxation behaviour in heterogeneous structures, were based on simple models, and solved the diffusive exchange problem analytically. Here a numerical simulation was performed using structures, based on randomly distributed spheres, which mimicked the experimental system closely. By introducing fluid particles into the system and applying a random walk algorithm the relaxation behaviour of these structures could be simulated. Then by generating a fluid velocity field, using a lattice Boltzmann simulation, the relaxation-resolved propagators, $P_\Delta\{Z;T_2\}$ were obtained. Comparisons of relaxation and T_2-resolved propagator simulations are made with experimental data.

2. Experimental

Calcium alginate beads of varying sizes (3, 1, and <1 mm) were studied. The 3 mm calcium alginate beads were made by dripping, under gravity, 2% w/v sodium alginate (medium viscosity—Sigma) solution into 0.2 M calcium chloride (Acros) solution. Here sodium ions were replaced with calcium ions, and bridges between alginate chains were created, forming a gel structure. The beads were left to equilibrate for several hours. The smaller beads were provided by Unilever Research and were produced using a similar method, where the sodium alginate solution was sprayed into the calcium chloride solution; the bead diameter was controlled by altering the droplet size of the spray [24]. The <1 mm beads were polydisperse, with a mean diameter of approximately 600 μm. T_1 relaxation times and self-diffusion coefficients (D), for the beads in a 0.1 M calcium chloride solution, were the same inside the gel beads and outside, in the pore fluid, giving values of 1.8 s and $2 \times 10^{-9}\,m^2\,s^{-1}$, respectively, at a temperature of 293 K. This indicated that the beads had an, essentially, unrestricted and uniform structure, which was expected for a 2% w/v hydrogel.

All NMR experiments were performed on a GE CSI Omega spectrometer equipped with a 2T horizontal wide-bore superconducting magnet. Magnetic field gradients were produced using Accustar S150 actively shielded gradient coils. A 100 mm diameter birdcage coil was used, with a typical 90° pulse length of 70 μs. Samples consisted of 22 mm internal diameter glass tubes, filled with the alginate beads in the centre with glass sintered disks on either side and a packing of glass beads at the ends. The pore fluid was 0.1 M calcium chloride solution. Transverse relaxation data were obtained using a slice selective CPMG sequence, typically using τ values of 5 ms and 1024 echoes, and exciting a slice of 10 mm in thickness. Relaxation time distributions were then obtained using two methods, a least squares fitting routine and an inverse Laplace transform program, CONTIN [25].

For the T_2-resolved propagator experiments, calcium chloride solution (0.1 M) was flowed through the samples using a Pharmacia P-50 HPLC pump at flow rates ranging from 7 to 14 ml/min. A schematic for the pulse sequence used is shown in Fig. 1. Typical parameters used in this experiment included a δ of 6 ms, Δ of 100 ms, $\mathbf{g}_{max}$ of 0.1 T/m and between 32 and 64 $\mathbf{q}$ encoding steps, depending on the flow rate. Parameters for the CPMG module were as given above for the one-dimensional relaxation measurements. This experiment produces a signal array, $S_\Delta(\mathbf{q}, t)$, where $\mathbf{q} = \gamma\delta\mathbf{g}/2\pi$ and $t = 2n\tau$, the CPMG sampling times. Fourier transformation of $S_\Delta(\mathbf{q}, t)$ with respect to $\mathbf{q}$ produces $S_\Delta\{Z; t\}$ and regularised Laplace inversion, using CONTIN, for each Z produces the T_2-resolved propagator $P_\Delta\{Z; T_2\}$. This

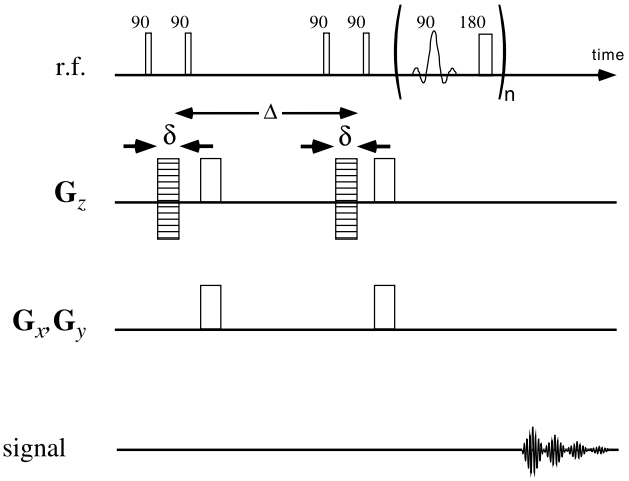

Fig. 1. Schematic RF and gradient pulse sequences for the T_2-resolved propagator experiment and is made up of a pulsed gradient stimulated (PGSTE) echo experiment followed by a CPMG train. The signal is put into the longitudinal plane prior to slice selection and phase information from the PGSTE sequence is recorded through phase cycling. A minimum of 16 phase cycles are required.

produces a two-dimensional plot of the natural log of the relaxation rate versus the displacement. Additionally, analysis of the Fourier transformed signal was performed using a least squares fitting program, which produced separate displacement propagators for the different relaxation components.

3. Simulations

3.1. Modelling the structure

A model of the bead pack was simulated using the program, NSCP3D [26], which is based on an algorithm developed by Jodrey and Tory [27] for generating close random packings of identical spheres. The packing was generated from a random distribution of points, which defined the centres of an inner and outer sphere whose diameters corresponded to a true and a nominal density, respectively. The program works to eliminate overlaps by moving the closest centres of spheres apart while gradually shrinking the outer diameter. The inner diameter, which defines the true density, is set to the minimum centre-to-centre distance after each iteration. The procedure terminates when the inner and outer sphere diameters coincide. The final packing fraction depends on the contraction rate of the outer sphere, and is variable, with a maximum possible packing fraction of 0.64. The array size used in this work was $128 \times 128 \times 128$, and periodic boundary conditions were imposed. Although, in principle, such boundary conditions can give rise to recorrelation effects [28], in the present context, where displacements are of the order of a bead diameter, we expect such effects to be minimal.

The size of beads and porosity were chosen to match the experimental alginate bead systems studied. For these simulations the porosity was 48.8% and the beads had a radius of 10 voxels. In the CPMG simulations the voxel length was defined as 0.15, 0.05, and 0.03 mm producing bead diameters of 3, 1, and 0.6 mm, respectively. In the T_2-resolved propagator experiment only a singe bead size was used, of diameter 1 mm and voxel length 0.05 mm. A uniform internal network has been assumed for the beads, where there was no hindrance to diffusion or exchange.

3.2. Determination of the velocity field

Once the bead matrix was generated the velocity field was produced using a lattice Boltzmann simulation. The lattice Boltzmann method has proved highly successful in simulating fluid flow through porous media [14,29]. The program used was written by Warren [30]. In this simulation a discrete form of the Boltzmann equation [31] was used, which was based on a $d3q15$ lattice, corresponding to 3 spatial dimensions and 15 velocity vectors. The initial conditions are of zero velocity and a uniform pressure gradient between two faces normal to the axis of flow. Boundary conditions at the bead surface were imposed using a bounce back convention. The simulation continued until the calculated mean velocity did not change appreciably.

3.3. Simulation of $P_\Delta\{Z;T_2\}$

The bead structure is seeded with 10^6 particles, which are allowed to flow and diffuse freely in and between pore and bead regions. The trajectories of these particles are measured and the environment they are in is recorded. The relaxation decay of the NMR signal can be determined by applying a probability algorithm that a spin will relax, which depends on the relaxation time of the region the spin is in. From this the relaxation and displacement behaviour of the system can be followed and so the propagator, $P_\Delta\{Z;T_2\}$ can be simulated. For simplicity a single intrinsic relaxation time of 40 ms has been used for fluid in the bead and 1.8 s for fluid in the pore, values which are representative of those determined for the experimental system. The simulation was run over the same time scales as the $P_\Delta\{Z;T_2\}$ experiment, i.e., with a 'PGSE' module of duration 100 ms followed by a relaxation module of duration 10 s. Sampling during the relaxation experiment was at intervals of 10 ms, corresponding to a τ value of 5 ms, as used in the experiments. The time step used throughout was 1 ms and the flow steps were calculated from the velocity field generated from the lattice Boltzmann simulation, which had an average velocity of $0.42\,\mathrm{mm\,s^{-1}}$. Diffusive steps were calculated using a diffusion coefficient of $2.2\times10^{-9}\,\mathrm{m^2\,s^{-1}}$. It should be noted that during the 'PGSE' module of the simulation, relaxation was turned off. This is because in the experiment, the system is sensitive to T_1 relaxation during this part, which was substantially longer than the observation time and was the same for the bead and the pore.

4. Results

4.1. T_2 Relaxation behaviour

Fig. 2 shows the T_2 relaxation distributions for the (A) 3 mm, (B) 1 mm, and (C) <1 mm alginate beads. These distributions were obtained using the inverse Laplace transform program CONTIN. Table 1 gives the modal T_2 values found for these distributions, along with the corresponding values found by least squares fitting using a sum of exponentials. As expected for a system in the slow diffusive exchange regime, we see multi-modal distributions [3]. The relaxation times associated with the modes fall into three groups—short (T_2 <30 ms), intermediate ($T_2\sim300$ ms), and long (T_2 >1 s). Although it is not possible to associate particular modes exclusively with physical regions within the system under conditions of slow exchange, earlier work by Booth and Packer [32] suggests that it is reasonable to regard the long and intermediate T_2 modes as arising predominately from fluid held within the pore. By the same token, the short T_2 modes may be largely associated with fluid held within the beads. The fact that we observe two (or in the case of the 0.6 mm beads, three) such modes suggests that the beads may have a heterogeneous structure, possibly arising from the manufacturing process. This structure is observable only when we acquire an effective zero-time point immediately after the first 90° pulse of the CPMG sequence and is not present in the two-dimensional $P_\Delta\{Z;T_2\}$ measurements (in which the first point is acquired at 2τ after the initial excitation) which form the main focus of this paper—we have therefore not investigated this matter further.

The combined intensity of the long and intermediate T_2 modes amounts to approximately 40% of the total in all the systems studied here, which provides an estimate of the porosity. Further support for this procedure for obtaining the porosity is provided by an analysis of simulated data where the porosity is known a priori, so that a direct comparison can be made between true porosity and that generated from the relaxation time distributions. The results of such an analysis are presented in Table 2 where they are compared with values obtained from the experimental data. As mentioned earlier, in performing the simulations we assigned a single relaxation time (40 ms) to the bead—we accordingly used a three-component least squares fitting procedure to analyse both the experimental and simulated

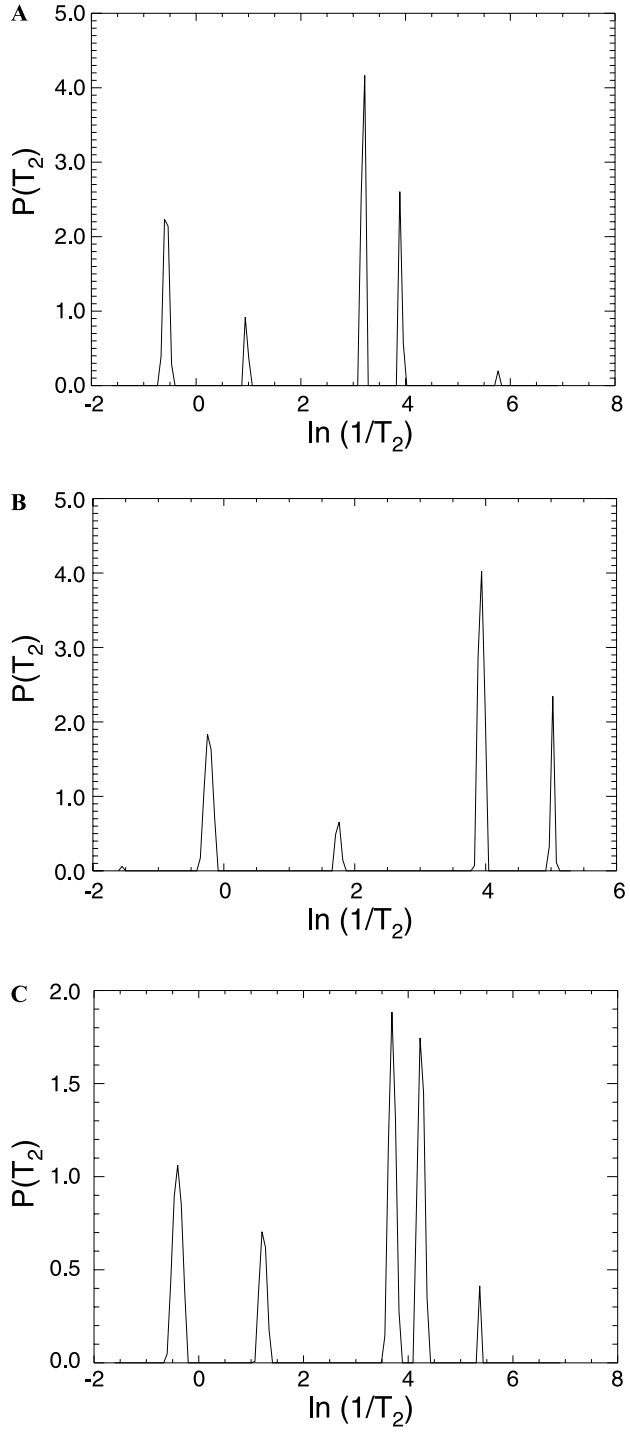

Fig. 2. T_2 relaxation time distributions for (A) 3 mm, (B) 1 mm, and (C) <1 mm alginate beads. Distributions were obtained using CONTIN with an input of 1000 echoes and an output of 128 points.

Table 1
CONTIN and least squares fitting analyses for experimental T_2 relaxation time distributions for (a) 3 mm, (b) 1 mm, and (c) <1 mm beads

	CONTIN fitting		Least squares fitting	
	$T_2(s)$	(%)	$T_2(s)$	(%)
(a)				
Peak 1	1.82	30.6	1.85	32.5
Peak 2	0.39	7.8	0.46	8.1
Peak 3	0.04	38.2	0.04	42.1
Peak 4	0.02	22.5	0.02	17.2
(b)				
Peak 1	1.82	29.4	1.91	28.0
Peak 2	0.32	10.7	0.37	11.7
Peak 3	0.02	52.8	0.02	47.8
Peak 4	0.01	7.1	0.01	12.5
(c)				
Peak 1	1.49	24.1	1.55	23.7
Peak 2	0.30	12.5	0.31	13.2
Peak 3	0.025	31.8	0.027	27.2
Peak 4	0.015	28.9	0.015	31.1
Peak 5	0.005	2.7	0.007	4.8

Table 2
Comparison of simulated and experimental T_2 relaxation time distributions for (a) 3 mm, (b) 1 mm, and (c) <1 mm beads, calculated using a three-exponential least squares fit

	Experimental data (least squares fitting)		Simulation data	
	$T_2(s)$	(%)	$T_2(s)$	(%)
(a)				
Peak 1	1.81	33.8	1.60	40.0
Peak 2	0.35	8.7	0.61	5.9
Peak 3	0.033	57.5	0.041	54.1
(b)				
Peak 1	1.89	28.4	1.34	35.7
Peak 2	0.34	12.1	0.38	11.0
Peak 3	0.019	59.5	0.041	53.3
(c)				
Peak 1	1.53	24.3	1.10	34.2
Peak 2	0.28	13.8	0.29	13.5
Peak 3	0.019	61.9	0.041	52.3

data. Reasonable agreement is seen between T_2 values for corresponding modes in the two datasets. It is evident that for the simulated data the true porosity (48.8%) is not reflected in the intensity of the long—T_2 component for any of the three bead sizes. However, summing the long and intermediate T_2 component intensities leads to values of 47.7, 46.7, and 45.9% for the 0.6, 1, and 3 mm beads, respectively—values which, while still underestimates, lie much closer to the true porosity. These data highlight the danger associated with measuring the porosity of such systems by using the relaxation time distributions. If the porosity is measured by taking only the long T_2 component, it will be underestimated, as there will be a contribution from the molecules held within the pore in the intermediate relaxation component.

We now turn to the T_2 values associated with each of the modes, first considering the values found for the simulated systems. For the 3 mm beads the T_2 value of

the long T_2 mode is close to that assigned to the bulk fluid phase and progressively decreases as with decreasing bead size whereas the shortest T_2 value is independent of bead size. Although the complexity of the system prevents us from drawing any quantitative conclusions from these observations, it is clear that they are consistent with a picture in which the relaxation times associated with the two extremal modes are, to a greater or lesser extent, dominated by the intrinsic values in the fluid and hydrogel phases, with the increasing opportunity for exchange as the beads become smaller resulting in a decrease in the long T_2 component. The fact that no corresponding increase is seen in the short T_2 component is simply a consequence of the fact that the rapid relaxation in the bead completely dominates the effects of exchange.

It is harder to interpret the behaviour of the intermediate T_2 component as this arises solely as a consequence of exchange and, we must assume, represents some form of average of the (in principle) infinite set of modes expected for a system in slow diffusive exchange. However, we note that the general trend towards increased intensity and reduced T_2 as the bead size decreases is consistent with the increasing importance of exchange mediated relaxation as the pore size decreases and the interfacial area between the phases increases. It is the behaviour of this intermediate peak, which is dependent on both the intrinsic relaxation times within the two phases and the morphology of the bead pack, which is of most interest in this study. The T_2 values obtained from the experimental data follow broadly the same trends as observed for the simulations. Differences between the simulations and experiments are possibly associated with differences in signal to noise ratios, with the simulated data having a higher S/N ratio, the internal structure of the gel beads not being perfectly unrestricted or uniform.

4.2. T_2-Resolved propagators

T_2-Resolved propagators are presented for the 3 mm beads (Fig. 3), 1 mm beads (Fig. 4), and <1 mm beads (Fig. 5) at average fluid flow velocities of 0.5 and 1.0 mm s^{-1}. Both contour and surface plots are shown. The basic structure of the propagator, $P_{\Delta}\{Z;T_2\}$, is the same for the three bead sizes. A single relaxation component, at short T_2, is observed for fluid largely associated within the beads, as no zero time point is used. This component has a Gaussian displacement distribution, centred about zero, typical for molecules undergoing diffusion only. For the long relaxation component, arising from molecules predominantly in the pore structure, the propagator is elongated along the direction of flow. These molecules are experiencing flow and diffusion and so their propagator is more like that of a flow propagator. It is the behaviour of the intermediate

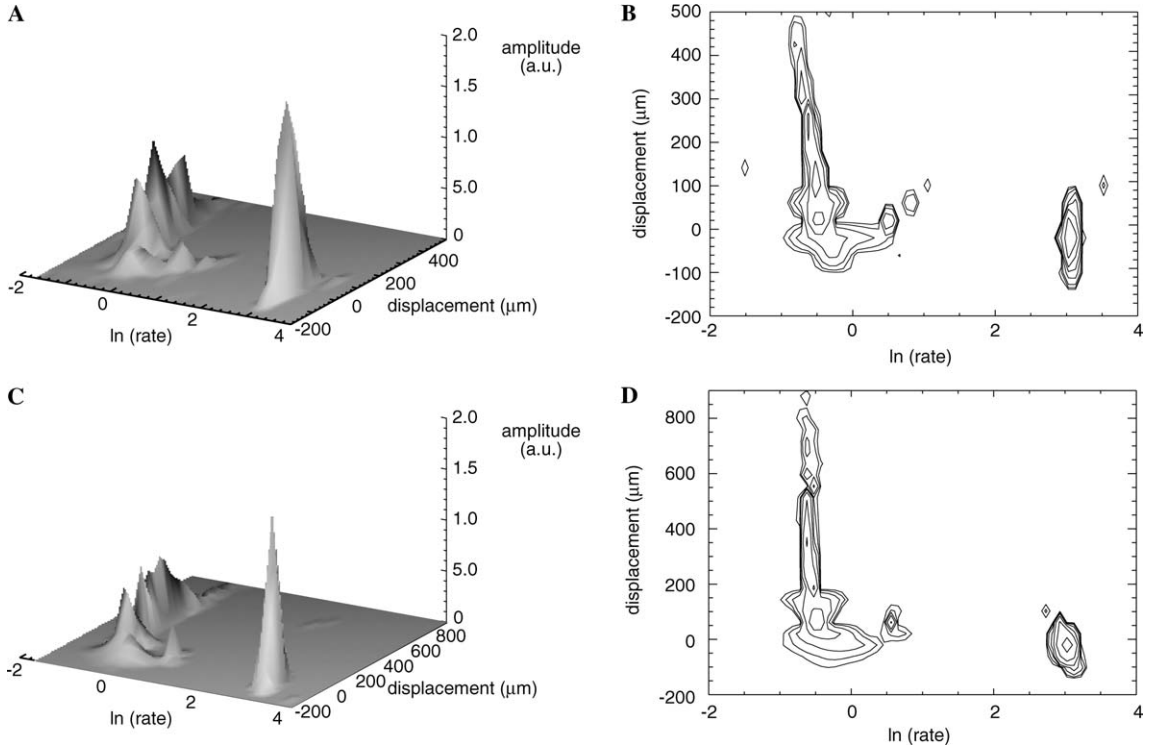

Fig. 3. Surface and contour plots of the T_2-resolved propagators, $P_{\Delta}\{Z;T_2\}$, for 3 mm beads at an average flow velocity of 0.5 mm s^{-1} (A,B) and 1.0 mm s^{-1} (C,D).

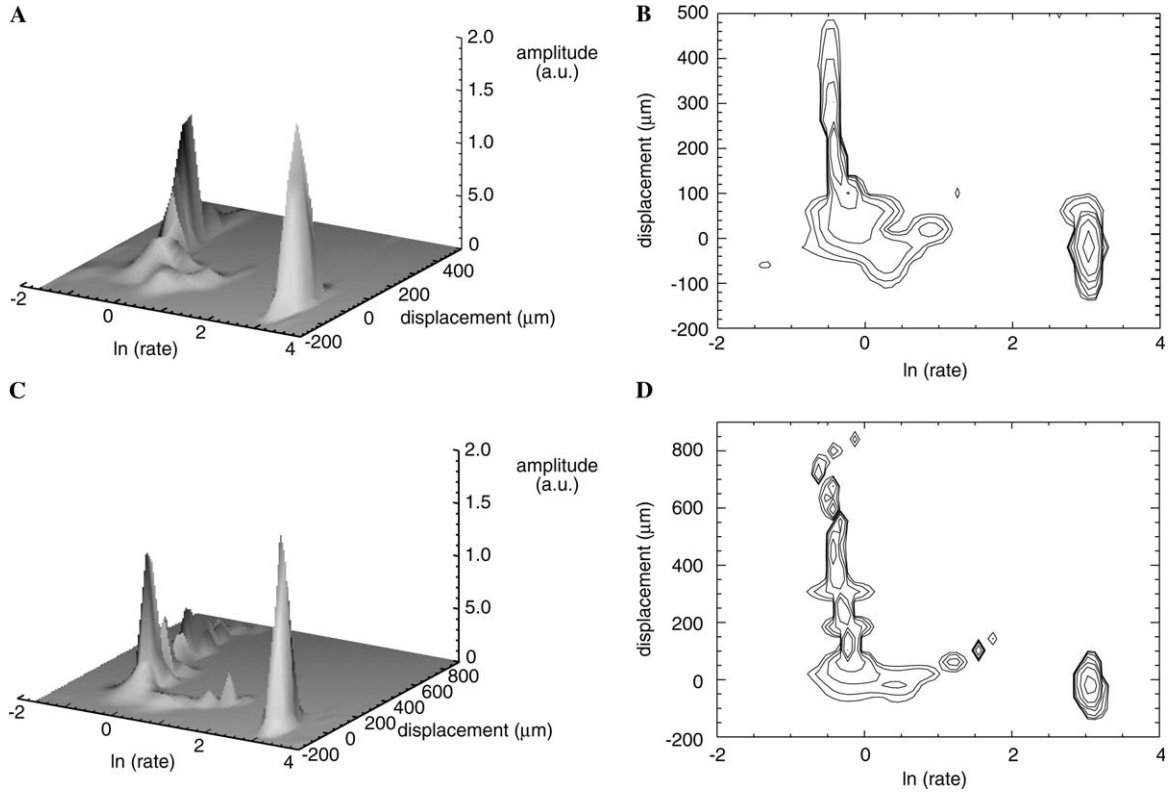

Fig. 4. Surface and contour plots of the T_2-resolved propagators, $P_\Delta\{Z;T_2\}$, for 1 mm beads at an average flow velocity of 0.5 mm s^{-1} (A,B) and 1.0 mm s^{-1} (C,D).

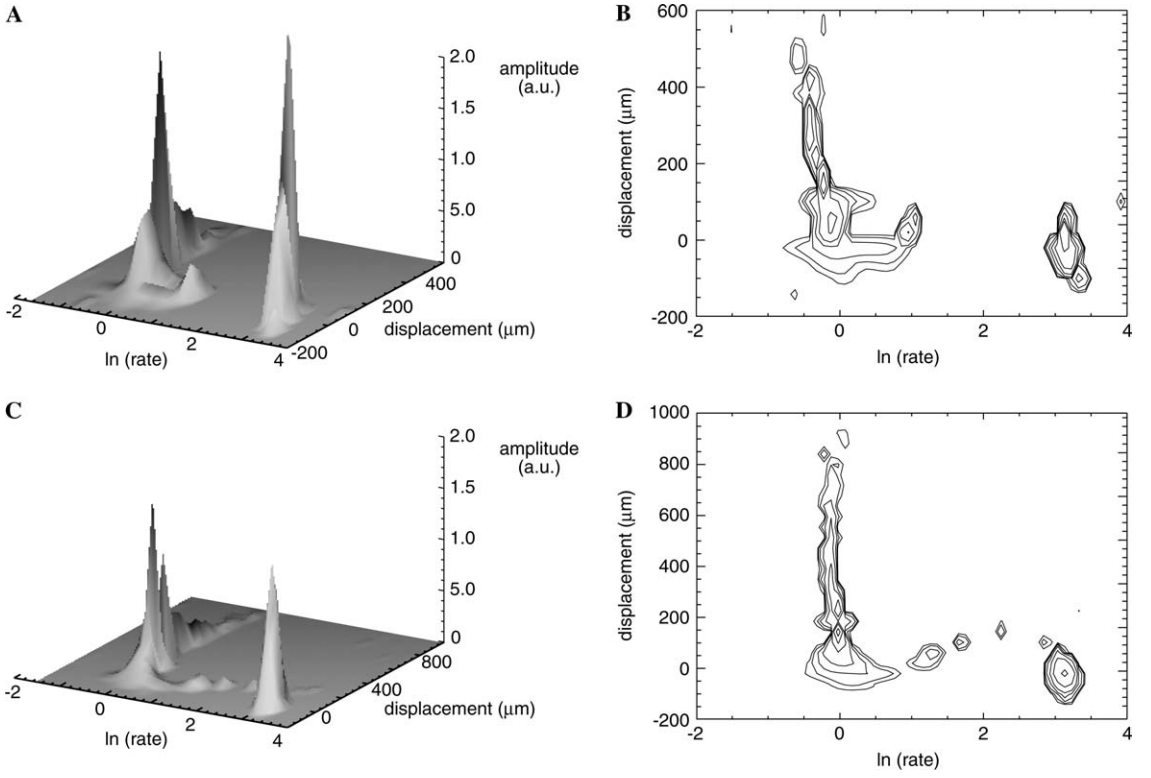

Fig. 5. Surface and contour plots of the T_2-resolved propagators, $P_\Delta\{Z;T_2\}$, for <1 mm beads at an average flow velocity of 0.5 mm s^{-1} (A,B) and 1.0 mm s^{-1} (C,D).

relaxation components that shows the most interesting behaviour and is found to be sensitive to bead size and flow rate. These intermediate relaxation components are found to vary in relaxation time with average displacement, with a collective trend of longer relaxation times correlating with smaller displacements. This variation of relaxation time and average displacement for the intermediate peaks is also seen to be affected by average flow rate. First, as expected, the maximum displacement for the intermediate peaks increases with the increased flow rate. What is also seen is that the number of intermediate peaks increases with increasing flow rate. These peaks also have a wider range of relaxation times. For the $P_\Delta\{Z;T_2\}$ propagators at lower flow rate the intermediate peaks have relaxation times closer to that of the bulk relaxation time. As the average flow rate is increased the peaks at larger displacement have significantly shorter relaxation times, which approach that of the relaxation time inside the bead. In the case of the 0.6 mm beads, at an average flow velocity of $1\,\mathrm{mm\,s^{-1}}$, the intermediate components span the relaxation times from those of the pore to those of the bead, over a displacement range of $\approx 200\,\mu\mathrm{m}$. Similar behaviour is observed in the 1 mm beads though it is not as pronounced. It can be argued that the longest and shortest relaxation components are associated with fluid remaining predominantly in the pore and bead, respectively. As noted earlier, this is a simplification, but in the slow diffusion regime, which is largely applicable to these systems, this may not be unreasonable. So if the intermediate peaks are to be considered as the spins that predominantly exchange between pores and beads then within this population there will be a range of exchange behaviour and hence flow and relaxation histories. By increasing the flow there appears to be greater resolution of the displacement and relaxation behaviour. Towards the other extreme where there is no flow, as in the bulk T_2 measurement, they average to a single value. However in the displacement-resolved experiment these exchanging populations can be resolved by their flow history and may possibly give us information on the relationship between the internal pore structure and transport processes.

From these observations of the intermediate relaxation components, it is tempting to associate larger average displacements with a higher probability of exchanging into the bead which acts as the volume relaxation sink. What the structure of these peaks suggests is that spins which are in smaller channels, and so have more probability of exchanging into the bead phase, are likely to have higher flow rate and hence higher displacement. This picture agrees with the observed peak distribution within the relaxation-resolved propagators. A correlation between pore size and velocity has been suggested by Sederman et al. [33], where they found that some small pores had higher average velocities than larger ones, though a direct correlation was complicated by other factors such as connectivity etc.

Such an interpretation is almost certainly an oversimplification and cannot be confirmed through analysis of the experimental results alone. To investigate this system further simulations have been undertaken and the results compared with experiment. The $P_\Delta\{Z;T_2\}$ propagator for simulations of a 1 mm bead structure is presented in Fig. 6. These simulated data agree well with those obtained experimentally. The simulated propagator displays very similar relaxation/displacement behaviour for the intermediate relaxation peaks, to that found in the experimental data. The simulated data however does however give rise to shorter T_2's for these peaks, though this can be explained possibly by the following differences between experiment and simulation. First, there is a greater signal to noise ratio for the simulated data than for the experimental data. Second, the simulated bead structure was simplified and a single relaxation time was used for the beads, where experimentally multi-exponential behaviour was found, and possibly this averaged value was shorter than the true

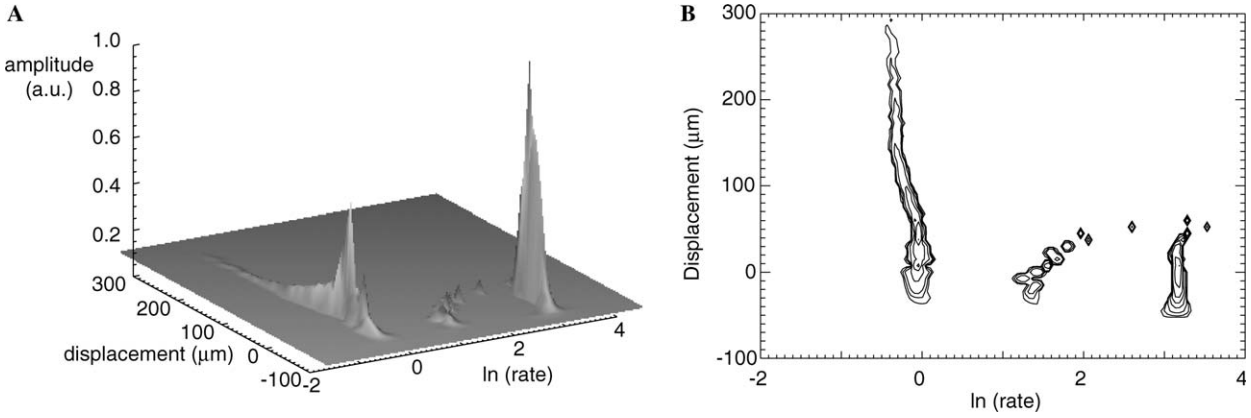

Fig. 6. Surface and contour plots of the T_2-resolved propagators, $P_\Delta\{Z;T_2\}$, for a simulation of the 1 mm bead system, with an average flow velocity of $0.42\,\mathrm{mm\,s^{-1}}$.

value for the fluid in the beads, particularly at the outer regions. Thirdly the internal structure of the beads may not be perfectly unhindered, as has been assumed. However, even with these slight differences, it can be seen that the simulations reproduce the experimental result and so in-depth analysis of fluid behaviour is possible through the interrogation of particle histories within the simulation. Using these simulations it is possible to follow the trajectory of individual particles and their exchange behaviour, and through this a correlation between transport through a smaller channel, where the probability of exchange is high, with faster moving channels might be possible. Investigations of this and the effects of changing the displacement observation time are still in progress and will be reported in a future publication.

In previous work, in which we reported the results of flow/T_2 correlation experiments for flow in packed bed of glass beads [21], we presented the results of an analysis of the NMR response expected for Poiseuille flow in a circular capillary when diffusion-to-surface is the dominant relaxation mechanism. That analysis, which is here presented in more detail in Appendix A, indicates that, in principle, it is possible for the propagators associated with relaxation modes higher than the zeroth to have regions of negative amplitude.

The analysis presented so far for the $P_{\Delta}\{Z;T_2\}$ propagators, in this paper, has used the inverse Laplace transform program CONTIN, with a constraint of positive amplitudes. Attempts to invert the data using CONTIN without the non-negativity constraint led to oscillatory solutions, which were clearly non-physical. In fact we are not aware of any reports in the literature where Laplace inversion of noisy data has been successfully accomplished, using either CONTIN or any other algorithm, without the constraint of non-negative amplitudes. By removing the negativity constraint the number of possible solutions significantly increases. To reduce the number of possible solutions and so find the correct one, it would be necessary to include another kind of constraint, but one that mimics the physics of the system more closely [34]. As yet, this is not possible. However the possibility of negativity, in the intermediate propagator, does suggest further analysis, where this can be taken into account. By unconstrained non-linear least-squares fitting we found that such negative regions could indeed be observed in the experimental data for the alginate bead packs. Here the signal decays are fitted to a maximum of three exponentials. The simulated data and experimental data, for the 1 mm beads, have been re-analysed using a least squares fitting routine and the relaxation resolved propagators are shown in Figs. 7 and 8, respectively. The change in T_2 relaxation time with displacement is also presented. Here negative amplitudes are clearly seen for the intermediate relaxation peak, as predicted by the theory. What should also be noted is that the same relaxation time/displacement trend of longer relaxation time with longer displacement and vice versa is also seen in the least squares fitting analysis of the simulated data. It is also seen in the 1 mm experimental data at the higher flow rate (1 mm s^{-1}). The experimental data are however more noisy.

It should be noted that there are some important differences between the alginate bead systems and glass bead/capillary systems. The alginate beads provide a volume sink and not a surface sink. Equally there will be molecules originating from the bead, which may exchange and so contribute to the intermediate peaks. Although there are significant differences between these, it is not, however, surprising that negative components should arise here also, as the underlying physics which

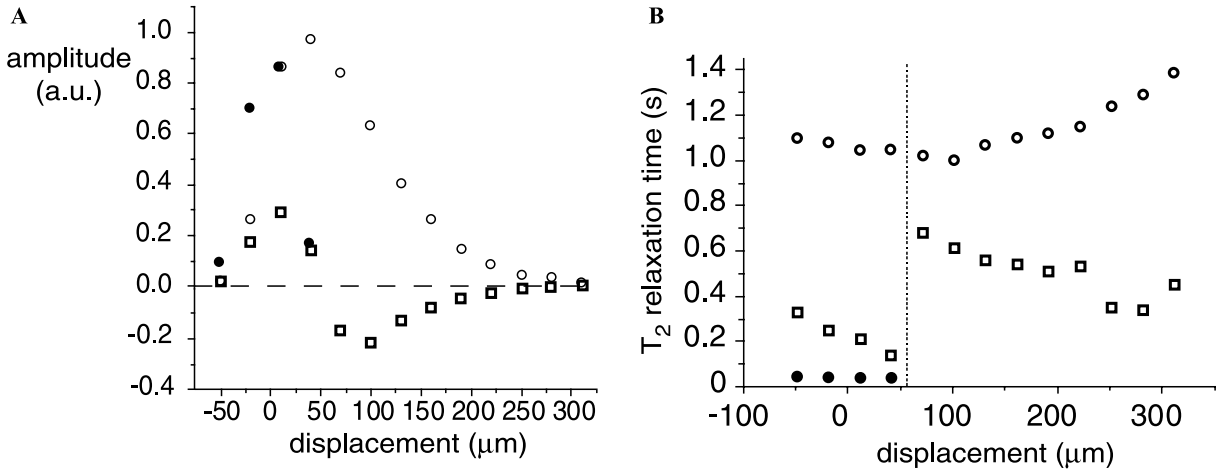

Fig. 7. Least squares fitting analysis of the simulated $S_{\Delta}\{Z,t\}$ for 1 mm at an average flow velocity of 0.42 mm s^{-1}. Plot (A) gives the resolved propagators for the long T_2 (○), intermediate T_2 (□), and short T_2 (●) components. Plot (B) shows the change in relaxation time with displacement for these three populations.

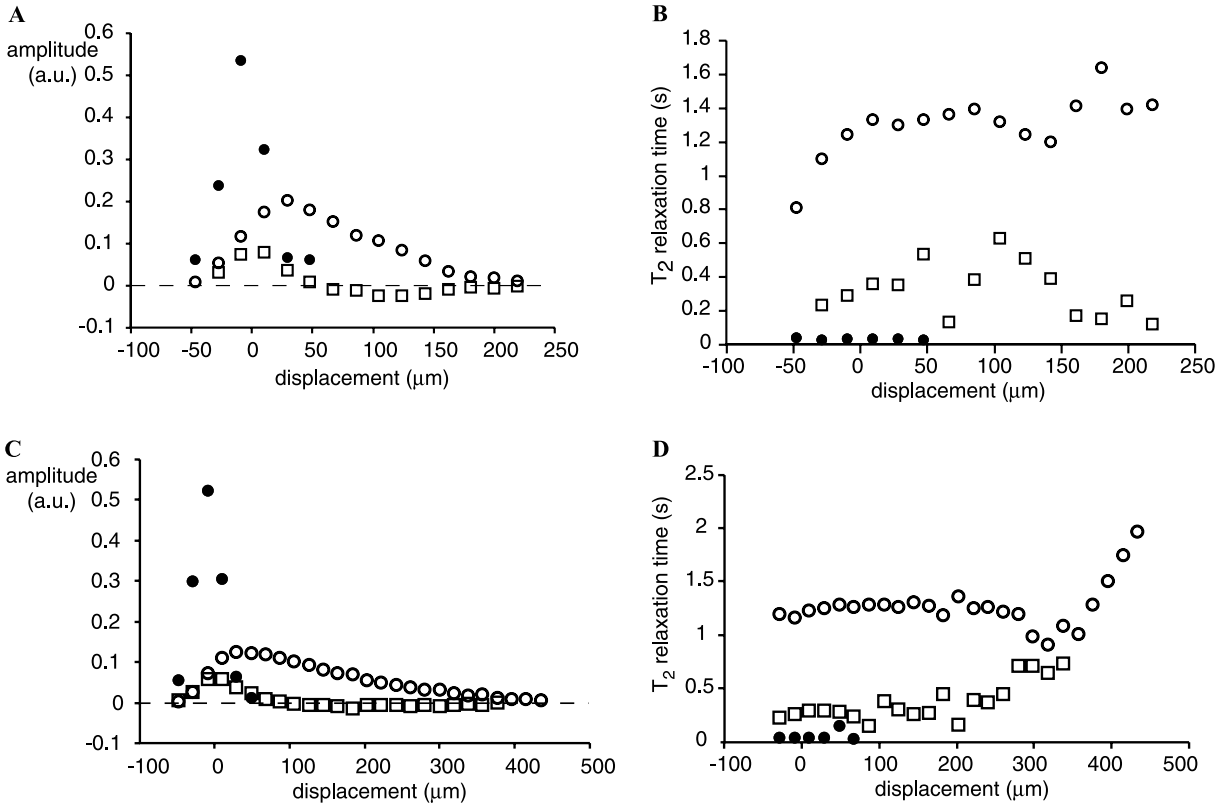

Fig. 8. Least squares fitting analysis of $S_{\Delta}\{Z,t\}$, for 1 mm at an average flow velocity of $0.5\,\mathrm{mm\,s^{-1}}$ (A,B) and $1.0\,\mathrm{mm\,s^{-1}}$ (C,D). Plots (A) and (C) give the resolved propagators for the long T_2 (○), intermediate T_2 (□), and short T_2 (●) components. Plots (B) and (D) show the change in relaxation time with displacement for these three populations.

leads to the appearance of such components is common to all three systems. We therefore acknowledge that a complete analysis of our data requires a relaxation of the non-negativity constraint in the Laplace inversion and we intend to continue to explore possibilities for accomplishing this; however, in the context of the present work, we believe our main conclusions remain valid despite the imposition of the non-negativity constraint. We also remark that, even were we able to allow for negative components, physical interpretation of their significance would remain difficult, through the extended Brownstein–Tarr analysis, because the intermediate-T_2 propagator observed is, presumably, some form of average of several (in principle, an infinite number of) higher modes.

Finally, we remark that the extended BT theory shows that the relaxation time of each mode is constant and independent of displacement. This is not seen in the case of the intermediate relaxation peaks in the $P_{\Delta}\{Z;T_2\}$ experiment, which vary in relaxation time depending on displacement. It is most likely that an explanation for this rests in the complex internal structure of the porous bead system. In the analytical solution a uniform diameter of capillary was used. This leads to a single value for the dimensionless parameter $\mu a/D$, where μ is the surface relaxivity, a the lengthscale, and D the diffusion coefficient. However, in the porous alginate bead system, spins which experience a flow-driven displacement, which is large compared to diffusive displacements, effectively 'sample' a range of length scales, leading to a displacement dependent value of the intermediate relaxation time. Possibly this range of pore length scales, could provide information on internal structures and transport processes through analysis of this intermediate component. To further understand this, interrogation of the simulations is required, as this negativity was also observed here.

5. Conclusions

The T_2-resolved propagator experiment has been used to probe the flow and exchange behaviour of water flowing through an alginate bead pack. By combining Pulsed Gradient Stimulated Echo (PGSTE) experiments with a Carr–Purcell–Meiboom–Gill we have been able to begin to unpack the average propagator into more individual spin histories. The two-dimensional propagators, while complex in nature, show some tantalising insight into the morphology and flow behaviour within these systems. In particular, the correlation we have observed between large displacements and short relax-

ation times in the intermediate T_2 component might suggest that fastest-flowing spins are present in relatively narrower channels in the bead-pack. The two-dimensional nature of our experiments provides a stringent test of our computer simulations, and the excellent agreement we observe between the two suggests that further refinement of the algorithms, which record individual spin-histories, may yield valuable insight, at the microscopic level, into fluid transport processes in these systems.

Acknowledgments

We thank Unilever for financial support and MMB thanks EPSRC for an Advanced Research Fellowship.

Appendix A

In this Appendix we give details of the extension of Brownstein and Tarr's treatment of diffusion-to-surface mediated relaxation. Brownstein and Tarr give the general form for evolution of nuclear magnetisation as:

$$\rho(r,t) = \sum_{k=0}^{\infty} C_k F_k(r)\, \exp(-t/T_k), \tag{A.1}$$

where $\rho(\mathbf{r},t)$ is the transverse nuclear magnetisation density and the $F_k(\mathbf{r})$ form a complete set of orthogonal functions over the region of interest. In their development of Eq. (A.1) Brownstein and Tarr assume that the initial density $\rho(\mathbf{r},0)$ is real and spatially uniform. However in our experiments, the effect of the PGSE sequence which precedes the CPMG pulse train is to impose a phase modulation on $\rho(\mathbf{r},0)$. The nature of the modulation depends on the displacement history during the observation time Δ of spins residing at $\mathbf{r}$ and on the wavevector $\mathbf{q}$ associated with the gradient pulses. We therefore write:

$$\rho(r,q,\Delta,t) = \sum_{k=0}^{\infty} C_k(q,\Delta)\mathrm{F}_k(r)\exp(-t/T_k), \tag{A.2}$$

where $\rho(\mathbf{r},q,\Delta,0)$ and the coefficients $C(\mathbf{q},\Delta)$ are to be regarded as complex quantities. From the orthogonality of the F_k it follows that:

$$C_k(q,\Delta) = \frac{\int_V F_k(r)\rho(r,q,\Delta,0)\,\mathrm{d}r}{\int_V F_k^2(r)\,\mathrm{d}r}, \tag{A.3}$$

where the integrations are to be performed over the bounded volume. The observed NMR signal $S(q,\Delta,t)$ is just the integral of ρ over that volume:

$$S(q,\Delta,t) = \sum_k \xi_k \int_V F_k(r)\rho(r,q,\Delta,0)\,\mathrm{d}r \exp(-t/T_k), \tag{A.4}$$

where:

$$\xi_k = \frac{\int_V F_k(r)\,\mathrm{d}r}{\int_V F_k^2(r)\,\mathrm{d}r}. \tag{A.5}$$

The initial density is:

$$\rho(r,q,\Delta,0) = \rho_0 \int P_\Delta(r|R)\,\mathrm{e}^{2\pi \mathrm{i} q r}\,\mathrm{d}R, \tag{A.6}$$

where ρ_0 is the magnetisation density at the beginning of the PGSE sequence and $P(\mathbf{r}|\mathbf{R})$ is the conditional probability density that spins residing at $\mathbf{r}$ at $t=0$ have undergone a displacement $\mathbf{R}$ during the observation time Δ. The observed NMR signal is therefore:

$$S(q,\Delta,t) = \sum_k \xi_k \int\int F_k(r)P_\Delta(r|R)e^{2\pi \mathrm{i} q r}\,\mathrm{d}r\,\mathrm{d}R \times \exp(-t/T_k). \tag{A.7}$$

Fourier transformation with respect to $\mathbf{q}$ now yields the direct space propagator $P_\Delta(\mathbf{R},t)$:

$$P_\Delta(R,t) = \sum_k \xi_k \int F_k(r)P_\Delta(r|R)\,\mathrm{d}r \exp(-t/T_k). \tag{A.8}$$

Thus least-squares fitting of the experimentally determined $P_\Delta(\mathbf{R},t)$ to a sum of exponentials yields the coefficients:

$$A_k(R,\Delta) = \xi_k \int F_k(r)P_\Delta(r|R)\,\mathrm{d}r. \tag{A.9}$$

For Pouseille flow in a cylindrical capillary the propagator can be expressed analytically if Taylor dispersion during the time Δ is neglected; it is then possible to solve for the A_k analytically:

$$A_k(R,\Delta) = \xi_k F_k\left(\sqrt{a^2 - \frac{Z}{K\Delta}}\right), \tag{A.10}$$

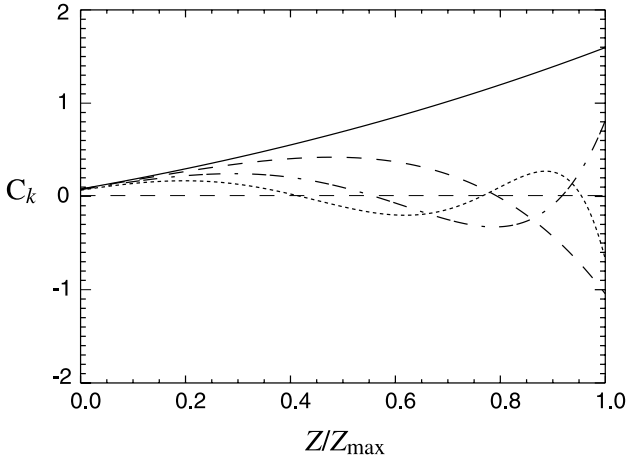

Fig. 9. Variation of the amplitudes, C_k, for the first 4 relaxation modes, $k=0$ ( ), $k=1$ (- - -), $k=2$ ($\cdots$), $k=(3$ — $\cdot)$, as a function of longitudinal displacement with parameters $M = 2\times10^{-4}\,\mathrm{m\,s^{-1}}$, $a = 10^{-4}\,\mathrm{m}$ and $D = 2\times10^{-9}\,\mathrm{m^2\,s^{-1}}$. Relaxation times for the modes $k=0,\ldots,3$ are, respectively, 1.052, 0.197, 0.0790, and 0.0418 s.

where a is the radius of the capillary, K is a constant which depends only upon the fluid viscosity and the pressure drop along the length of the capillary and Z is the displacement along the length of the capillary experienced by spins at radial coordinate $\mathbf{r}$.

For cylindrical geometry Brownstein and Tarr give the F_n terms of the cylindrical Bessel functions J_n as $J_0\varepsilon_k\mathbf{r}/a$ where the ε_k are the positive roots of the transcendental equation $\varepsilon_k J_1(\varepsilon_k)/J_0(\varepsilon_k) = Ma/D$; M and D are, respectively, the surface relaxivity and the self-diffusion coefficient. In Fig. 9 we show illustrative plots of the coefficients $C_k(\mathbf{R}, \Delta)(k = 0, \ldots, 3)$ for $Ma/D = 10$. Fig. 9 shows the variation of amplitudes for the first 4 relaxation modes, as a function of longitudinal displacement for this case.

References

[1] E.J. Fordham, A. Sezginer, L.D. Hall, Imaging multiexponential relaxation in the $(y, \mathrm{Log}_e T_1)$ Plane, with application to clay filtration in rock cores, J. Magn. Reson. A 113 (1995) 139–150.

[2] A.T. Watson, C.T.P. Chang, Characterising porous media with NMR methods, Prog. Nucleic. Magn. Reson. Spectroc. 31 (1997) 343–386.

[3] K.R. Brownstein, C.E. Tarr, Importance of classical diffusion in NMR studies of water in biological cells, Phys. Rev. A 19 (1979) 2446–2453.

[4] P.S. Belton, B.P. Hills, The effects of diffusive exchange in heterogeneous systems on NMR line shapes and relaxation processes, Mol. Phys. 61 (1987) 999–1018.

[5] B.P. Hills, K.M. Wright, P.S. Belton, NMR studies of water proton relaxation in Sephadex bead suspensions, Mol. Phys. 67 (1989) 193–208.

[6] B.P. Hills, J.E.M. Snaar, Water proton relaxation studies of pore microstructure in monodisperse glass bead beds, Mol. Phys. 84 (1995) 141–157.

[7] J.E.M. Snaar, B.P. Hills, Water proton relaxation studies of air-water distributions in beds of randomly packed monodisperse glass microspheres, Mol. Phys. 86 (1995) 1137–1156.

[8] P.T. Callaghan, A. Coy, T.P.J. Halpin, D. MacGowan, K.J. Packer, F.O. Zelaya, Diffusion in porous systems and the influence of pore morphology in pulsed gradient spin echo nuclear magnetic resonance studies, J. Chem. Phys. 97 (1992) 651–662.

[9] P.T. Callaghan, A. Coy, D. MacGowan, K.J. Packer, F.O. Zelaya, Diffraction-like effects in nmr diffusion studies of fluids in porous solids, Nature 351 (1991) 467–469.

[10] K.J. Packer, J.J. Tessier, The characterisation of fluid transport in a porous solid by pulsed gradient stimulated echo NMR, Mol. Phys. 87 (1996) 267–272.

[11] L. Lebon, J. Leblond, J.P. Hulin, Experimental measurement of dispersion processes at short times using a pulsed field gradient NMR technique, Phys. Fluids 9 (1997) 481.

[12] L.L. Latour, R.L. Kleinberg, P.P. Mitra, C.H. Sotak, Pore-size distributions and tortuosity in heterogeneous porous media, J. Magn. Reson. A 112 (1995) 83–91.

[13] D. van Dusschoten, P.A. Dejager, H. Van As, Extracting diffusion constants from echo-time-dependent PFG NMR data using relaxation-time information, J. Magn. Reson. A 116 (1995) 22–28.

[14] B. Manz, P. Alexander, P.B. Warren, L.F. Gladden, Characterisation of fluid through porous media using three-dimensional microimaging and pulsed gradient stimulated echo NMR, Magn. Reson. Imaging 16 (1998) 673–675.

[15] S. Stapf, K.J. Packer, R.G. Graham, J.-F. Thovert, P.M. Adler, Spatial correlations and dispersion for fluid transport through packed glass beads studied by pulsed field-gradient NMR, Phys. Rev. E 58 (1998) 6206–6221.

[16] D. van Dusschoten, C.T.W. Moonen, P.A. de Jager, H. Van As, Unraveling diffusion constants in biological tissue by combining Carr–Purcell–Meiboom–Gill imaging and pulsed field gradient NMR, Magn. Reson. Med. 36 (1996) 907–913.

[17] B.P. Hills, K.M. Wright, J.E.M. Snaar, Dynamic NMR q-space studies of microstructure with the multigrade CPMG sequence, Magn. Reson. Imaging 14 (1996) 305–318.

[18] Y. Song, L. Venkataramanan, M.D. Hürlimann, M. Flaum, P. Frulla, C. Straley, T_1–T_2 Correlation spectra obtained using a fast two-dimensional Laplace inversion, J. Magn. Reson. 154 (2002) 261–268.

[19] P.T. Callaghan, S. Godefroy, B. Ryland, Use of the second dimension in PGSE NMR studies of porous media, Magn. Reson. Imaging 21 (2003) 243–248.

[20] P.T. Callaghan, S. Godefroy, B. Ryland, Diffusion-relaxation correlation in simple pore structures, J. Magn. Reson. 162 (2003) 320–327.

[21] M.M. Britton, R.G. Graham, K.P. Packer, Relationships between flow and NMR relaxation of fluids in porous solids, Magn. Reson. Imaging 19 (2001) 325–331.

[22] M.D. Hürlimann, Effective gradients in porous media due to susceptibility differences, J. Magn. Reson. 131 (1998) 232–240.

[23] L. van der Weerd, S.M. Melnikov, F.J. Vergeldt, E.G. Novikov, H.V. As, Modelling of self-diffusion and relaxation time NMR in multicomponent systems with cylindrical geometry, J. Magn. Reson. 156 (2002) 213–221.

[24] W.J. Sime, Food Gels (1990) 67.

[25] S.W. Provencher, Contin: a general purpose constrained regularization program for inverting noisy linear algebraic and integral-equations, Comput. Phys. Commun. 27 (1982) 229–242.

[26] M. Bargiel and J. Moscinski, *NSCP3D*, (1989) (source code obtained from the CLRC web site at http://www.dl.ac.uk/CCP/CCP5/librar.html).

[27] W.S. Jodrey, E.M. Tory, Computer simulation of close random packing of equal spheres, Phys. Rev. A 32 (1985) 2347–2351.

[28] D. Kandhai, U. Tallarek, D. Hlushkou, A. Hoekstra, P.M.A. Sloot, H. Van As, Numerical simulation and measurement of liquid hold-up in biporous media containing discrete stagnant zones, Philos. Trans. R Soc. Lond. A Math. Phys. Eng. Sci. 360 (2002) 521–534.

[29] B. Manz, L.F. Gladden, P.B. Warren, Flow and dispersion in porous media: lattice-Boltzmann and NMR studies, AIChE 45 (1999) 1845–1854.

[30] P.B. Warren, Electroviscous transport problems via lattice-Boltzmann, Int. J. Mod. Phys. C 8 (1997) 889–898.

[31] G.R. McNamara, G. Zanetti, Use of the Boltzmann equation to simulate lattice-gas automata, Phys. Rev. Lett. 20 (1988) 2332–2335.

[32] A.D. Booth, K.J. Packer, Magnetic spin lattice relaxation in the presence of spin-diffusion. The one-dimensional, two-region system, Mol. Phys. 62 (1987) 811–828.

[33] A.J. Sederman, M.L. Johns, P. Alexander, L.F. Gladden, Structure-flow correlations in packed beds, Chem. Eng. Sci. 53 (1998) 2117–2198.

[34] Y. Song, Schlumberger-Doll Research, Connecticut (2003).